

Multistability and Paradoxes in Lossy Oscillator Networks

Robin Delabays,^{1,*} Saber Jafarpour,^{1,2} and Francesco Bullo¹

¹*Center for Control, Dynamical Systems, and Computation,
UC Santa Barbara, Santa Barbara CA 93106-5070, USA.*

²*School of Electrical and Computer Engineering,
Georgia Institute of Technology, Atlanta GA 30332-0250, USA.*

**Corresponding author (robindelabays@ucsb.edu).*

(Dated: February 5, 2022)

The analysis of dissipatively coupled oscillators is a challenging problem with high stakes in actual applications, such as large scale physical systems. Many standard mathematical methods are not applicable to such systems, due to the lack of symmetry of the network induced by dissipative couplings. Here we emphasize that the synchronization of coupled oscillators can be equivalently interpreted as the problem of flow distribution over a network. Based on these equivalent interpretations, we demonstrate a close correspondence between multiple stable synchronous states and *winding cells* in systems of dissipatively coupled oscillators. The recently introduced notion of winding cells, associated to a graph, forms a natural winding partition of the n -torus and capture essential characteristics of synchronous states in lossless systems. Leveraging the winding partition of the n -torus, we provide algorithms to compute the synchronous solutions of general networks of coupled oscillators. Furthermore, we identify three paradoxical behaviors of lossy networked systems, to be contrasted with the behavior lossless systems. Namely, we show that loop flows and dissipation can increase the system's transfer capacity, and that dissipation can promote multistability.

Keywords: coupled oscillators, complex networks, dissipation, synchronization, flow networks, energy systems

Synchronization of networked oscillators and the distribution of flows over a power grid are equivalent formulations of the same problem. Over the last decades, major advances in our understanding of such phenomena were obtained under the approximation of lossless flows. However, when dealing with realistic systems, power flows are subject to resistive losses or, equivalently, coupled oscillators are subject to frustration. Based on graph theory adapted to the n -torus, we propose a mathematical formulation for the analysis of lossy oscillator networks. Furthermore, we identify some paradoxical behaviors in these networks and analyze them through our framework. Our work contributes to the long history of the analysis of multistability in power systems.

Synchronization and flow networks. The history of scientific investigation about synchronization is traditionally traced back to Huygens' observation of an "odd kind of sympathy" in the XVIIth century [1, Vol. 5, p. 246]. It is however only in the last decades that a tractable framework has been developed [2–4], thanks in particular to the pioneering works of Winfree in the 1960s [5], and Kuramoto in the 1970s-80s [6, 7]. Shortly thereafter, the problem of synchronization has been embedded in the framework of network systems [8–10], first based mostly on numerical simulations, evolving progressively towards more and more analytical results [2, 4, 11]. Even in the simplest form of coupled oscillators, the interplay between dynamics and network structures leads to rich and sometimes unexpected behaviors.

The interactions between synchronizing oscillators is naturally interpreted as a flow of information or commodity between the nodes of a network. This dual interpretation of synchronization and flows is instrumental in understanding the emerging phenomenon of synchronization. In systems of rotating masses connected by springs, the interactions is precisely the force exerted by the springs on the different masses [11, Fig. 1]. The change in a mass' position is then related to the imbalance of forces it is subjected to. In high voltage power grids [12], a rotating turbine in a plant accumulates kinetic energy and accelerate if all the power it produces is not transmitted to its neighboring buses. In motion planning [13, 14], agents adapt their trajectory with respect to relative position of other agents. The rate of change of an oscillator's state is then determined by the imbalance of the commodity received from or sent to its neighbors. When the interactions or flows of commodity balance out at each agent, such that all agents have identical rate of change, then the relative positions of the agents are constant in time: we say that they are *synchronized*. There is then a direct link between synchronized states of coupled oscillator networks and the distribution of flows on a graph. The natural way a commodity is dispatched over a network can be puzzling, to say the least. It remains challenging and fascinating to understand the interplay between the complex network structures and the nontrivial interactions between sources and sinks of this commodity.

Lossless oscillator networks. One of the simplest models of synchronization considers a set of oscillators, each described by a phase $\theta \in \mathbb{S}^1 \simeq [-\pi, \pi)$, interacting with each other through a 2π -periodic coupling, function

of their phase difference $h: [-\pi, \pi) \rightarrow \mathbb{R}$,

$$\dot{\theta}_i = \omega_i - \sum_{j=1}^n a_{ij} h_{ij}(\theta_i - \theta_j), \quad i \in \{1, \dots, n\}. \quad (1)$$

In the context of commodity flows, the *natural frequencies* $\omega_i \in \mathbb{R}$ correspond to commodity in- and outputs. The system evolves on the n -torus $\mathbb{T}^n = (\mathbb{S}^1)^n$ and the underlying network structure is determined by the coefficients $a_{ij} \in \{0, 1\}$. These coefficients are nonzero if and only if oscillators i and j interact. The oscillators are *frequency synchronized* (or *phase locked*) if, at some point in time, $\theta_i = \dot{\theta}_j$, for all i, j . The intrinsic compact nature of each oscillator's domain and the continuity of the coupling function require h_{ij} to be nonlinear, and periodic in the systems of interest here. Whereas linear networked systems are well-understood [15], the nonlinear nature of the coupling between oscillators can lead to rich and intricate behaviors [12].

The vast majority of the literature about synchronization of coupled oscillators assumes symmetric couplings, i.e., two coupled oscillators influence each other with the same strength. In the flow network interpretation, symmetric couplings correspond to lossless flows, i.e., the flow of commodity between i and j contributes with equal magnitude and opposite sign to each end of the edge between i and j . Shortly put in mathematical terms, $h_{ij}(x) = -h_{ji}(-x)$. Consequences of this strong relation between h_{ij} and h_{ji} are in particular: (i) conservation of the total flow in the system, simplifying the calculation of the asymptotics of Eq. (1) and; (ii) symmetry of the Jacobian matrix of the system, guaranteeing nice and convenient spectral features. The properties of systems with lossless couplings allowed to derive a long list of results about their dynamics, namely, conditions for existence and uniqueness of their synchronous states [11, 16, 17], multistability [12, 18], and clustering [19, 20], to name but a few. An approach, common to various works, is to design a fixed-point iteration [16–18], whose convergence is guaranteed under some convexity properties of the *energy landscape* of the system [21, 22].

Challenges in the lossy systems. However, while the lossless assumption is reasonable in many cases, it is often not realistic and can lead to inaccurate predictions (e.g., see the power flow problem in the Discussion and the Methods Sections). In the flow interpretation, the transfer of a commodity is subject to "dissipation" (under the form of friction, resistance, leaks, data loss) or "frustration" (e.g., as phase lag), meaning that the amount sent from i to j is strictly larger than the amount received by j from i . The importance of understanding the more realistic case of dissipative couplings motivated the early work by Sakaguchi and Kuramoto [23, 24] and is still an active field of research. Recent numerical investigations [25, 26] as well as analytical studies in regular systems [27–29] are beginning to shed light on a more

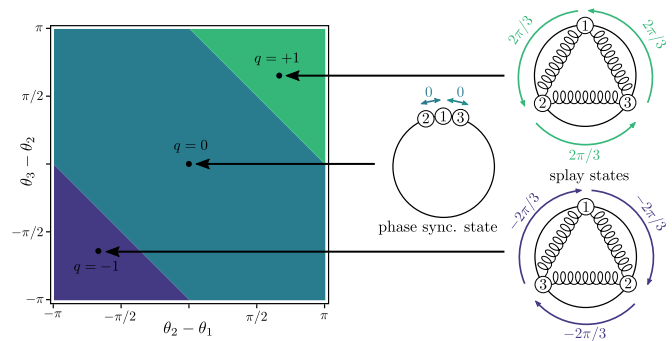


FIG. 1. Projected winding cell partition of the 3-torus (left) and representation of three equilibria of a spring network (right). Points on the 3-torus are projected on the 2-dimensional space of angular differences $\theta_2 - \theta_1$ and $\theta_3 - \theta_2$. A winding number $q \in \mathbb{Z}$ is associated to each equilibrium, counting the number of times its angles wind counterclockwise around the origin. The three dots (left) are equilibria of the spring network, labeled with their winding numbers q . The *phase synchronous state* has all angles identical and therefore $q = 0$. Equilibria with $q = \pm 1$ are the so-called *splay states*. The colored areas in the left panel represent the set of points with same winding number, i.e., the winding cells, forming a partition of the 3-torus.

in-depth understanding of dissipative networks. More generally, the extension of standard approaches to more realistic systems is gaining momentum in the fields synchronization and complex networks [30–32].

An additional outstanding challenge is that, up to this day, it is unclear to what extent the properties enjoyed by lossless networks are preserved in more realistic, dissipative systems. In the global scientific aim of a faithful modeling of real systems, it is of utmost importance to decipher the impact of dissipation in standard models of networked dynamics. Indeed, conditions for existence, uniqueness, and multiplicity of synchronous states or for the emergence of clustering in lossless systems [11, 12, 18–20] are yet to be adapted to their dissipative counterpart. Furthermore, it is now largely documented [33] that phase frustration can lead to the occurrence of *solitary* and *chimera states* [26, 34–37], that are extensively studied, but still only partially understood.

Understanding dissipative systems is challenging for a number of reasons. In such systems, flow conservation is lost and the linearization of the system typically loses its symmetry. Furthermore, while Eq. (1) can be formalized as a gradient system over an energy landscape when $h_{ij} = -h_{ji}$, this property immediately fails in dissipative systems. Therefore, technical approaches based upon energy landscapes are not applicable any longer. Incorporating dissipation in the system even requires to re-think the intuitive vectorial formulation of Eq. (1), in order to recognize the directionality of flows. Notice that, surprisingly, even a clear vectorial form of the dissipative dynamics is lacking in the literature.

Objectives and contributions. Our aim is to develop an analysis framework to characterize the location, properties, and stability of synchronous solutions of dissipative oscillator networks. In the task of globally characterizing synchronous states of lossless oscillator networks, an instructive and effective approach has been to leverage the concepts of *winding numbers* and *winding cells* [18]. Given a cycle of oscillators $\sigma = (\theta_1, \dots, \theta_{|\sigma|}, \theta_1)$, the associated winding number $q_\sigma(\boldsymbol{\theta})$ counts the number of times the oscillators' angles wrap around the origin when following σ (a rigorous definition is given in the Results Section). A winding cell is a subset of the n -torus \mathbb{T}^n whose points have the same winding number around each cycle. Winding cells form a partition of the n -torus (the *winding partition*) and directly result from the network structure of the system and from the compact nature of the oscillators' domain. The concepts of winding numbers and winding cells are illustrated in Fig. 1. Note that winding cells are well-defined in dissipative systems, because they depend only on the network structure. It is however still unclear if the relation between stable synchronous states and winding cells, established in Ref. [18] for lossless systems, is valid.

There are two main contributions in this manuscript. First, we identify and detail some surprising and paradoxical behaviors of dissipative oscillator systems, that have escaped analysis up to this day. Specifically, we show that, in some cases, increased dissipation can lead to more robust and more stable systems. We emphasize the link between these paradoxes and the winding cells where they occur. Therefore, we argue that the winding partition provides a clear phase portrait for the analysis of such behaviors. Motivated by these first observations, we proceed to the second contribution of this manuscript. Namely, we provide an analytical, statistical, and computational understanding of the solutions of dissipative flow problems. In particular, we show that, exactly as in lossless networks, there is at most one solution of the dissipative flow problem in each winding cell. This at most uniqueness property is rigorously proven for a small amount of dissipation and verified numerically for a wide range thereof. Furthermore, we provide a complete understanding of lossy systems on acyclic networks and give an algorithm computing the unique solution, if it exists. For general, cyclic graphs, we provide an iteration map that, under technical assumptions, converges to the unique solution in a given winding cell.

Overall, in this manuscript, we illustrate our findings with the *Kuramoto-Sakaguchi model* (see the Methods section and Refs. [8, 23, 24]). This model is particularly appealing in our context because it is a natural extension of the (lossless) Kuramoto model, and the amount of dissipation in the coupling can easily be tuned with a continuous parameter, namely the phase frustration $\phi \in \mathbb{R}$. Nevertheless, our analytical results are valid for a much broader class of coupling functions h_{ij} , that might be of

interest to the dynamical systems and network science communities.

Remark. *In addition to the demonstrations provided, the framework proposed here is naturally suited to the analytical study of networked dynamical system with directed interactions. For sake of conciseness and clarity, we limit our focus to dissipative interactions over undirected edges, but the framework covers naturally any type of directed interactions. We discuss these generalizations to a greater extent in the Discussion section.*

RESULTS

After a formal definition of the winding partition of the n -torus, we provide a careful description of a series of unexpected behaviors of dissipative oscillator networks. This section culminates with our rigorous mathematical results. A detailed formalism can be found in the Methods section and proofs are deferred to the Supplementary Information.

Algebraic graph theory on the torus.

Our framework is largely inspired by Ref. [18, Sec. 3]. The states of the system of Eq. (1) are points $\boldsymbol{\theta}$ in the n -torus \mathbb{T}^n , each component being a point θ_i of the circle \mathbb{S}^1 . Comparing points on \mathbb{S}^1 requires to define angular differences, which is somewhat arbitrary. In this manuscript, we use the *counterclockwise difference*

$$d_{cc}(\theta_1, \theta_2) = \text{mod}(\theta_1 - \theta_2 + \pi, 2\pi) - \pi \in [-\pi, \pi). \quad (2)$$

Intuitively, the counterclockwise difference is a projection of the angular difference on the interval $[-\pi, \pi)$.

Given a cycle $\sigma = (i_1, \dots, i_{|\sigma|}, i_1)$ in a graph \mathcal{G} (see Methods for details), one can calculate the *winding number* around cycle σ associated with the state $\boldsymbol{\theta} \in \mathbb{T}^n$,

$$q_\sigma(\boldsymbol{\theta}) = (2\pi)^{-1} \sum_{j=1}^{|\sigma|} d_{cc}(\theta_{i_j}, \theta_{i_{j+1}}) \in \mathbb{Z}. \quad (3)$$

Three states with different winding numbers are illustrated in Fig. 1 for the 3-cycle. Intuitively, the winding number counts the number of times the angles in $\boldsymbol{\theta}$ wind around the origin when following the cycle σ . Then, given a cycle basis $\Sigma = \{\sigma_1, \dots, \sigma_c\}$ of the graph, we naturally define the *winding vector* associated to a state $\boldsymbol{\theta} \in \mathbb{T}^n$,

$$\mathbf{q}_\Sigma(\boldsymbol{\theta}) = [q_{\sigma_1}(\boldsymbol{\theta}), \dots, q_{\sigma_c}(\boldsymbol{\theta})]^\top \in \mathbb{Z}^c. \quad (4)$$

Nonzero winding numbers are typically associated to *loop flows* [18, 38, 39], i.e., a commodity flow of constant magnitude around a cycle of the network. Such loop flows occupy line capacity, but do not deliver commodity anywhere.

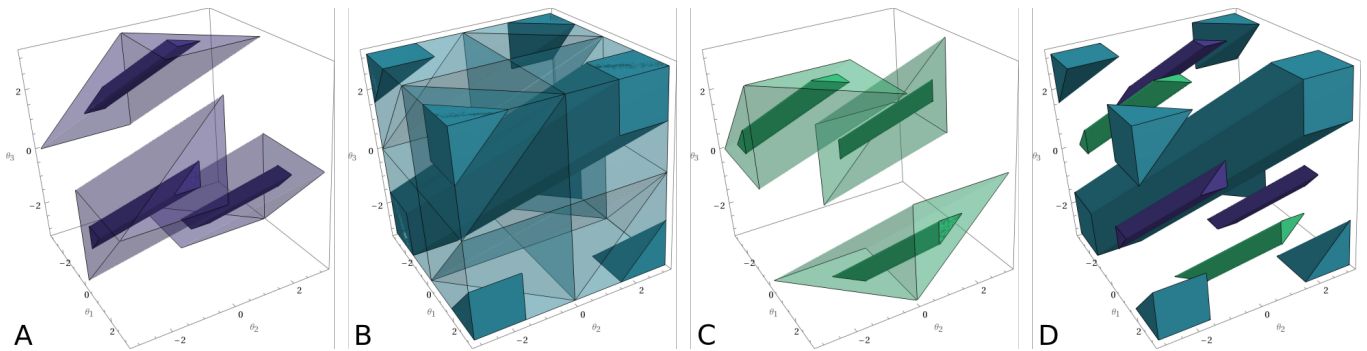


FIG. 2. Winding cells and their cohesive subsets, for a cycle of length $n = 3$. The 3-dimensional plots shows the unfolded 3-torus, where each dimension parametrizes one of the three angles and the winding cells become polytopes. The sides of the cube have then to be considered as identified (left-right, top-bottom, front-back). (A) The transparent volume is $\Omega(+1; \sigma)$, the winding cell of winding number $q = +1$, and the solid volume is the $3\pi/4$ -cohesive set, i.e., the subset of $\Omega(+1; \sigma)$ where the counterclockwise differences do not exceed $3\pi/4$. (B) The transparent volume is $\Omega(0; \sigma)$, the winding cell of winding number $q = 0$, and the solid volume is the $\pi/2$ -cohesive set. (C) The transparent volume is $\Omega(-1; \sigma)$, the winding cell of winding number $q = -1$, and the solid volume is the $3\pi/4$ -cohesive set. (D) Union of the cohesive sets of the previous panels. A key result of this manuscript is that there is at most one solution to Eq. (1) in a certain cohesive subset of each winding cell, i.e., in each solid volume.

Remark. *The winding number is a natural extension to complex networks, of the quantification of vortex flows in regular lattices, that arise in statistical physics (e.g., superfluids [40] or superconductors [41]). As far as we can tell, the notion of winding numbers in systems of coupled oscillators can be traced back to Refs. [42, referee discussion] and [43].*

For a graph with c cycles, a winding vector $\mathbf{u} \in \mathbb{Z}^c$ can be uniquely associated to each state in \mathbb{T}^n . Therefore we can define the *winding cell* associated with winding vector \mathbf{u} ,

$$\Omega(\mathbf{u}; \Sigma) = \{\boldsymbol{\theta} \in \mathbb{T}^n : \mathbf{q}_\Sigma(\boldsymbol{\theta}) = \mathbf{u}\}. \quad (5)$$

The counterclockwise difference is bounded, and so are the winding numbers. There is then a finite number of winding cells for a given graph \mathcal{G} , forming a finite partition of \mathbb{T}^n . See Fig. 2 for an illustration of winding cells in a cycle of $n = 3$ oscillators.

Paradoxical behaviors of dissipative systems

Three unexpected behaviors of lossy oscillator networks are illustrated in Fig. 3 for the Kuramoto-Sakaguchi model. The first one is a direct extension of a phenomenon already noted for lossless systems. The two other have not been reported to the best of our knowledge.

Paradox 1: Loop flows increase capacity. First, one would expect the presence of a loop flow (i.e., nonzero winding number) to reduce the transmission capacity of the system, because lines are occupied by the aforementioned loop flow. In Figs. 3C and 3F, we see that the solutions with larger winding numbers tolerate larger com-

modity transfer. Even though such observations have been documented in the past for lossless systems [18, 44], it remains somewhat counterintuitive.

Paradox 2: Dissipation increases capacity. Second, an initial reasoning would suggest that increasing dissipation would reduce the robustness and reliability of a system. Indeed, if part of the transmitted commodity is lost on the way, then more of it needs to be injected and the system is operated closer to criticality. However, the relation between dissipation and robustness is not that simple, as we illustrate in Fig. 3C. Indeed, for a nonzero winding number, the ability of the system to synchronize can evolve non-monotonously with respect to the dissipation (see solution at $q = -1$). Such phenomenon is quite unexpected and, to the best of our knowledge, has not been reported so far.

Paradox 3: Dissipation promotes multistability. Different flow solutions differ by a collection of loop flows [38], i.e., for some solutions, the lines are more loaded than for others. Similarly as in the previous paradox, one would expect that increased dissipation would prevent the occurrence of loop flows and therefore of multiple solutions. However, according to Fig. 3F, a system with low dissipation ($\phi \in [0, 0.3]$) and low injection ($p \approx 0$) can have fewer solutions than more loaded and dissipative systems. Indeed, one would assume that lower loads and lower frustration leads to a larger margin of freedom in the system. Apparently, this is not necessarily the case and this can be attributed to the underlying network structure.

The paradoxical behaviors identified above are typically related to the coexistence of different solutions. As we show in this manuscript, there is a strong and direct link between different solutions and the winding partition

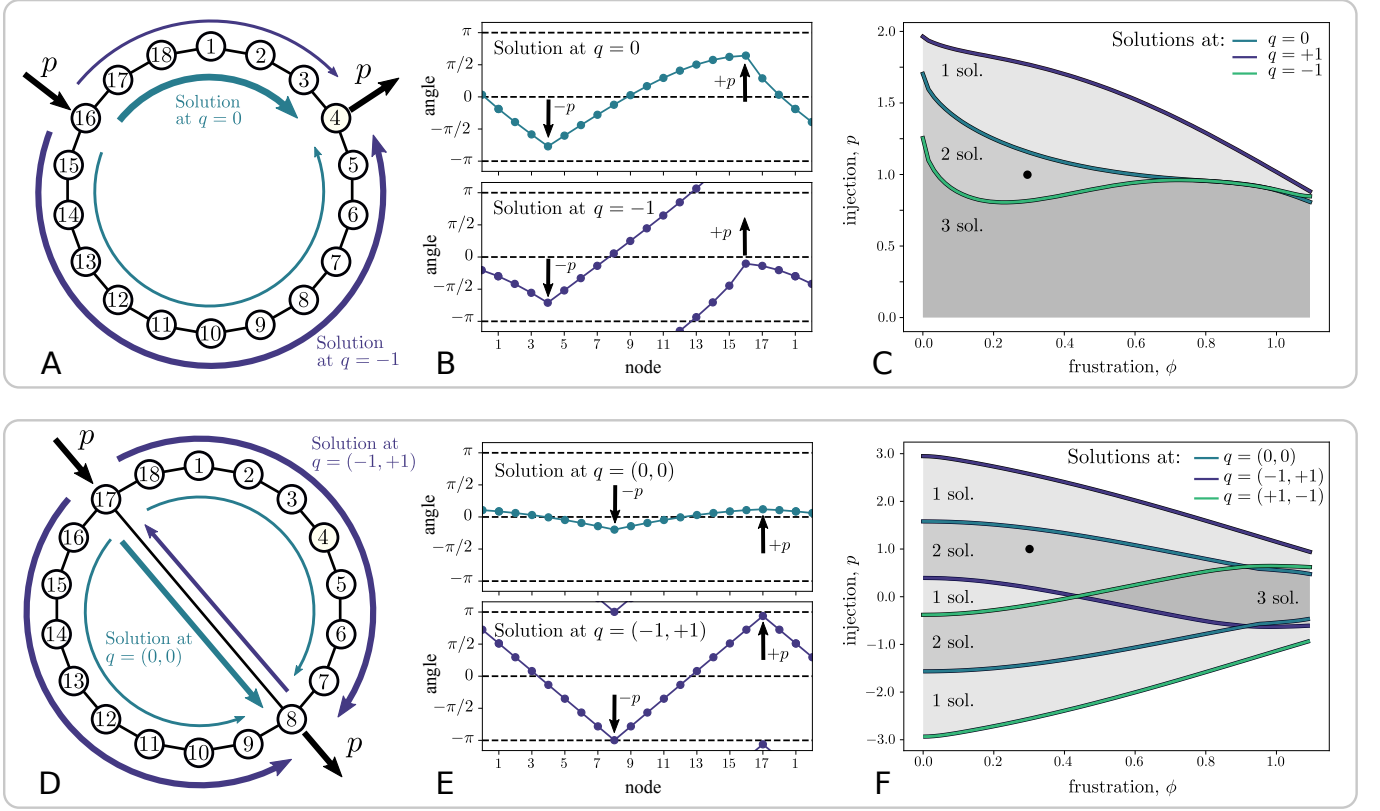


FIG. 3. Illustration of the paradoxical behaviors identified for the Kuramoto-Sakaguchi model on a cycle network (A, B, C) and a 2-cycle network (D, E, F), with unit coupling weights. (A) Qualitative distributions of flows over a cycle of $n = 18$ oscillators, with commodity injection $+p$ (resp. withdrawal $-p$) at node 16 (resp. 4). The arrows of two different colors visualize different flow solutions, with different winding numbers. (B) Angles corresponding to the two solutions of (A). One clearly sees that, for the solution at $q = +1$, the angles wrap around the circle, but not in the solution at $q = 0$. (C) Boundaries (colored curves) of the existence regions for solutions at different winding numbers, in the parameter space of phase frustration ϕ and injection magnitude p . The solutions in (A, B) were obtained for $(\phi, p) = (0.3, 1.0)$. The darkness of each area in the parameter space represents the number of existing synchronous states. It is surprising that (i) the solution at $q = +1$, i.e., with larger winding number, can carry a larger flow than the solution at $q = 0$, and (ii) for the solution at $q = -1$, the maximal tolerated commodity injection is not monotone in the frustration. (D, E, F): Same (A, B, C) respectively, for the 2-cycle network in (D). (F) Surprisingly, this network has fewer solutions for light load and frustration, $(\phi, p) \approx (0.0, 0.0)$, rather than for larger parameter values, e.g., $(\phi, p) = (0.3, 1.0)$.

of the n -torus.

Problem setup and solution: Synchronous states with dissipative couplings

We now formalize the problem of flow distribution in dissipative networks and present our main formal results. We provide a summary of the main notation symbols in the Methods Section (Table I).

Problem setup. Let \mathcal{G} be the undirected graph describing the interactions in of Eq. (1). Each edge $e = \{i, j\}$ of \mathcal{G} is endowed with two coupling functions, h_{ij} and h_{ji} , one for each orientation. For each edge, we choose an arbitrary orientation, say (i, j) . We will refer to the coupling functions as $h_e = h_{ij}$ and $h_{\bar{e}} = h_{ji}$, with \bar{e} denoting edge e with reversed orientation.

In our framework, Eq. (1) can be written in vectorial form as

$$\dot{\boldsymbol{\theta}} = \boldsymbol{\omega} - B_o \mathbf{h}(B^T \boldsymbol{\theta}), \quad (6)$$

using the incidence matrix B and the out-incidence matrix B_o induced by the chosen orientation. Both matrices are defined in the Methods Section, Eqs. (24) and (28) respectively. The coupling function $\mathbf{h}: \mathbb{R}^m \rightarrow \mathbb{R}^{2m}$ relates a vector of angular differences over the m undirected edges to the flows that are distinct for each edge orientation, hence \mathbf{h} has $2m$ components,

$$[\mathbf{h}(\mathbf{y})]_e = h_e(y_e), \quad [\mathbf{h}(\mathbf{y})]_{e+m} = h_{\bar{e}}(-y_e). \quad (7)$$

The edge indices $e \in \{1, \dots, m\}$ follow the orientation induced by the incidence matrix B . We refer to the discussion about the Kuramoto-Sakaguchi model in the Meth-

ods Section for an instructive example of the construction of Eq. (6).

From now on, it will be convenient to formulate the problem in terms of angular difference variables $\Delta \in \mathbb{R}^m$, rather than in terms of angle variables $\theta \in \mathbb{R}^n$. Constructing the vector of angular differences Δ from a vector of angles θ is straightforward, using the transpose of the incidence matrix, $\Delta = B^\top \theta$. The other direction however is not that direct. Indeed, from a difference vector Δ , one can recover the associated angle vector θ over a spanning tree of the graph. Now, the angular difference vector is consistent with the graph structure only if some *cycle constraints*. Namely, over the remaining edges of the graph $e = \{i, j\}$, that are not in the spanning tree, the constraint is $\theta_i - \theta_j = \Delta_e + 2\pi k$, $k \in \mathbb{Z}$. The integer multiple of 2π does not matter because the angles are compact variables over \mathbb{S}^1 . Mathematically speaking, these cycle constraints can be formalized using the *cycle-edge incidence matrix* C_Σ associated to a cycle basis $\Sigma = (\sigma_1, \dots, \sigma_c)$ [formally defined in the Methods section, Eq. (26)]

$$C_\Sigma \Delta = 2\pi \mathbf{u}, \quad (8)$$

for some winding vector $\mathbf{u} \in \mathbb{Z}^c$.

From now on, we will search for stable synchronous states of Eq. (6). Formally, we assume that, in a neighborhood of the origin, both h_e and $h_{\bar{e}}$ are strictly increasing, and for each edge e of \mathcal{G} , we require $|\Delta_e| \leq \gamma_e$, such that $h'_e(\Delta_e), h'_{\bar{e}}(-\Delta_e) > 0$. Following Gershgorin Circles Theorem [45, Theorem 6.1.1], under these assumptions, the spectrum of the system's Jacobian matrix lies in the left complex half-plane. The vector of angular differences is then restricted to the hypercube

$$R(\gamma) = \bigcap_{e \in \mathcal{E}} [-\gamma_e, \gamma_e] \subset \mathbb{R}^m. \quad (9)$$

The set of points $\theta \in \mathbb{T}^n$ whose angular differences along the edges of \mathcal{G} are in $R(\gamma)$ is referred to as a γ -cohesive set. The solid volumes in Fig. 2 show the intersections of the various winding cells of a 3-cycle and $R(\gamma)$ for different values of γ_e .

Gathering the above observations, we formulate the following problem, whose solutions are in one-to-one correspondence with synchronous states of Eq. (6).

Problem statement (Dissipative Flow Network). *Given a connected graph \mathcal{G} with n nodes, m edges, and cycle basis Σ , a vector of natural frequencies $\omega \in \mathbb{R}^n$, and appropriate coupling functions $h_e, h_{\bar{e}}$, associated to each edge e , find a solution $\Delta \in R(\gamma)$ of*

$$B_o \mathbf{h}(\Delta) - \omega = \varphi \mathbf{1}_n, \quad (10a)$$

$$C_\Sigma \Delta = 2\pi \mathbf{u}, \quad (10b)$$

for some synchronous frequency $\varphi \in \mathbb{R}$ and winding vector $\mathbf{u} \in \mathbb{Z}^{m-n+1}$.

In contrast with previous works on lossless systems, the flow map h_e is not odd, meaning that we do not impose the constraint $h_e(\theta_i - \theta_j) = -h_{\bar{e}}(\theta_j - \theta_i)$, hence our need of the out-incidence matrix B_o instead in Eq. (10a). Note that, even though in our example of the Kuramoto-Sakaguchi model all coupling functions are identical, in full generality, we allow $h_e \neq h_{\bar{e}}$.

Solution for acyclic graphs. In the case where \mathcal{G} is acyclic, we show that there is at most a unique solution to the Dissipative Flow Network Problem. Here there are obviously no cycle constraint and thus Eq. (10b) is trivially satisfied.

Theorem 1. *Consider the Dissipative Flow Network Problem on a connected acyclic undirected graph \mathcal{G} . Then there is at most one $\Delta \in R(\gamma)$ that satisfies Eq. (10a).*

The proof of Theorem 1 proceeds recursively and we provide it in the Supplementary Information. An implementation of an algorithm deciding the existence of the unique solution is provided online [46].

Remark. *Theorem 1 is the dissipative version of [18, Theorem 2.2]. The spirit of Theorem 1 is somewhat similar to Ref. [25, Sec. V], even though therein, the authors restrict their investigation to the Kuramoto-Sakaguchi model and cannot extend their approach to more general couplings.*

Solution for general graphs. The presence of cycles in the network can induce the existence of multiple solutions to the Dissipative Flow Network Problem (see Fig. 3 or [25]). We rigorously show here that winding vectors characterize these solutions for *sufficiently moderate dissipation*.

To do so, we define the *flow mismatch iteration* S_ϵ over the space of angular differences \mathbb{R}^m , whose fixed points are exactly the solutions of Eq. (10a). Namely, let

$$S_\epsilon: \mathbb{R}^m \rightarrow \mathbb{R}^m \quad (11)$$

$$\Delta \mapsto \Delta - \epsilon B^\top L^\dagger (B_o \mathbf{h}(\Delta) - \omega),$$

where $\epsilon > 0$ is a small step size and L^\dagger is the pseudoinverse of the graph Laplacian matrix. The flow mismatch iteration S_ϵ updates the vector of angular differences according to the mismatch between the input/output of commodities ω and the distribution of flows that corresponds to the current angular differences. It has two major properties:

- (I) the vector $\Delta^* \in R(\gamma)$ is a fixed point of S_ϵ if and only if it is a solution of Eq. (10a);
- (II) the map S_ϵ leaves each winding cell invariant, because $C_\Sigma B^\top = \mathbf{0}$. It means that fixing the winding vector of the initial conditions, imposes the winding vector of the fixed point of S_ϵ , if ever it exists.

One of the main lessons from Ref. [18] is that differential solutions of the flow network problem on the n -torus are better understood when put in the context of their winding cell. Accordingly, and thanks to the property (II) above, we split the Dissipative Flow Network Problem in each winding cell of the n -torus induced by the network structure. Fixing a winding vector $\mathbf{u} \in \mathbb{Z}^{m-n+1}$, we are guaranteed that if the initial conditions Δ_0 satisfy Eq. (10b), then each following iteration $\Delta_{k+1} = S_\epsilon(\Delta_k)$ will satisfy it as well.

We summarize the above observations in the following theorem, whose proof is a direct consequence of the compactness of $R(\gamma)$.

Theorem 2. *If the flow mismatch iteration S_ϵ is contracting, then there is at most one synchronous state of Eq. (1) in each winding cell.*

In what follows, we provide sufficient conditions for contractivity of S_ϵ . For each edge e of \mathcal{G} , we need to decompose the pair of coupling functions $(h_e, h_{\bar{e}})$,

$$h_{\text{od},e}(x) = [h_e(x) - h_{\bar{e}}(-x)]/2, \quad (12)$$

$$h_{\text{ev},e}(x) = [h_e(x) + h_{\bar{e}}(-x)]/2. \quad (13)$$

One can verify that $h_{\text{od},e}$ (resp. $h_{\text{ev},e}$) is an odd (resp. even) function and that $h_e = h_{\text{od},e} + h_{\text{ev},e}$. Intuitively, $h_{\text{ev},e}$ quantifies to what extent the coupling is dissipative. In the particular case where the coupling is lossless [i.e., $h_e(x) = -h_{\bar{e}}(-x)$], then $h_{\text{ev},e} = 0$.

Equipped with this decomposition of the couplings, we define two state dependent matrices, for $\mathbf{x} \in R(\gamma)$:

- (a) the *odd weighted Laplacian*, which is the Laplacian matrix of \mathcal{G} weighed by the derivatives of the odd parts

$$L_o(\mathbf{x}) = B \cdot \text{diag}[h'_{\text{od},e}(x_e)] \cdot B^\top. \quad (14)$$

We emphasize that the choice of orientation for each edge e does not matter in the definition of L_o . Also, the graph \mathcal{G} being connected and the coupling functions being strictly increasing implies that λ_2 , the smallest nonzero eigenvalue of L_o is necessarily positive;

- (b) the *even weighted degree matrix*, which is the diagonal matrix weighted by the absolute derivatives of the even parts,

$$[D_e(\mathbf{x})]_{ii} = \sum_{e \in E_i} |h'_{\text{ev},e}(x_e)|, \quad (15)$$

where E_i is the set of (undirected) edges incident to node i . The diagonal terms of D_e quantify the dissipativity of the couplings. In particular, for lossless couplings, $D_e = 0$.

Example. *In the case of the Kuramoto-Sakaguchi model, the coupling functions are*

$$h_e(x) = h_{\bar{e}}(x) = \sin(x - \phi) + \sin \phi, \quad (16)$$

and trigonometric identities yield

$$\begin{aligned} h_{\text{od},e}(x) &= \cos \phi \sin x, \\ h_{\text{ev},e}(x) &= \sin \phi (1 - \cos x), \end{aligned} \quad (17)$$

which we illustrate in Fig. 5B. We clearly see here the relation between $h_{\text{ev},e}$ and the dissipativity or frustration of the coupling. When $\phi = 0$, we recover the original Kuramoto model, where the coupling is lossless, and $h_{\text{ev},e} = 0$.

We are now ready to formulate the main theorem of this work. It clearly separates the impact of network connectivity, that promote the contractivity of S_ϵ , and of the dissipation, that works against contractivity of S_ϵ . We defer the proof to the Supplementary Information.

Theorem 3. *Given a Dissipative Flow Network Problem, define the odd weighted Laplacian L_o and the even weighted degree matrix D_e . If, for all $i \in \{1, \dots, n\}$,*

$$\sup_{\mathbf{x} \in R(\gamma)} (D_e)_{ii} < \inf_{\mathbf{x} \in R(\gamma)} \lambda_2(L_o), \quad (18)$$

then there exists a sufficiently small step size $\epsilon > 0$ such that the flow mismatch iteration S_ϵ [Eq. (11)] is contracting.

The left-hand-side of Eq. (18) quantifies the amount of dissipation that is "seen" at each node of the network, which vanishes for lossless couplings. The right-hand-side accounts both for the strength of the coupling between each pair of oscillators, through the weights, and for the connectedness of the graph, λ_2 being the *algebraic connectivity* [47]. Under our assumptions [\mathcal{G} is connected, couplings are strictly increasing on $R(\gamma)$], the right-hand-side of Eq. (18) is necessarily positive. For couplings with *sufficiently low dissipation*, Eq. (18) is then satisfied, which, combined with Theorem 2, yields the following corollary.

Corollary 4. *If Eq. (18) is satisfied, then there is at most a unique synchronous state of Eq. (1) in each winding cell. The number of synchronous states is then bounded from above by the number of winding cells.*

Theorem 3 and Corollary 4 give a rigorous, even though conservative, sufficient condition for the at most uniqueness of synchronous states in each winding cell. However, computing the eigenvalues of the odd weighted Laplacian can be time consuming. We therefore propose some lower bounds on $\lambda_2(L_o)$ in the Supplementary Information that are state-independent and may ease the verification of Eq. (18). The bounds are adapted from standard results of algebraic graph theory. The proofs are given in the Supplementary Information, Prop. 7.

DISCUSSION

Theorem 1 and Corollary 4 rigorously prove that, in each winding cell of the n -torus, there is at most a unique synchronous solution for dissipative networks of oscillators. In acyclic networks, the whole n -torus is trivially the unique winding cell, and there is therefore at most one solution to the Dissipative Flow Network problem (Theorem 1), independently of the amount of dissipation. For systems over more general, cyclic graphs, the winding partition provides a natural decomposition of the n -torus in subsets containing at most one solution. These results are a straight generalization of Ref. [18] to dissipative systems.

Even though the relation established in Corollary 4 is formally valid for relatively small amounts of dissipation, numerical experiments did not lead to any counterexample. Indeed, we empirically observed for a large range of network structures, frustration parameters, and initial conditions, that the flow mismatch iteration S_ϵ [Eq. (11)] can always be made contracting by taking a sufficiently small value of $\epsilon > 0$. We therefore conjecture that Corollary 4 is rather conservative and that the at most uniqueness property therein is valid for a much broader range of dissipation-to-coupling ratio. Furthermore, the comparison between coupling and dissipation in Eq. (18) clearly pinpoints how dissipation works against synchronization.

Both the proofs of Theorem 1 and Corollary 4 are algorithmic by nature. Namely, the proof of Theorem 1 considers recursively the flows on the edges of the acyclic graph, and Corollary 4 relies on the iteration map S_ϵ [Eq. (11)]. It is therefore straightforward to actually implement the proofs as routines, which we provide online [46].

The paradoxes illustrated in Fig. 3 emphasize that the introduction of dissipation in the coupling between oscillators has a nontrivial and surprising impact of the dynamics. The fact that both loop flows and dissipation can increase the transmission capacity of a system (Paradoxes 1 and 2) is arguably counterintuitive. We remark that both Paradoxes 1 and 2 occur for solutions with nonzero winding numbers ($q = +1$ and $q = -1$ respectively). It is also quite unexpected that more loaded and dissipative systems can possess more flow network solutions for a given network structure (Paradox 3). Again, this last paradox involves solutions in different winding cells. All paradoxes identified in Fig. 3 are strongly linked to solutions with nontrivial winding numbers. A general and thorough description of the different operating states of dissipative networks of oscillators then requires to tackle these systems through the prism of the winding partition.

The last decades have seen a large scale effort of the complex systems community to provide an analytical description of the power flow equations and of their solu-

tions (see the Methods Section). In 1972 already, Korsak showed [42] that, mathematically speaking, the power flow equations tolerated multiple solutions on cyclic networks. Since then, there has been a plethora of evidence, both analytical and numerical, that the power flow equations allow the coexistence of different solutions [12, 48–51]. Even some "real-world" events advocate in this direction [52, 53]. However, a large proportion of the work mentioned above relies on the *lossless line assumption*, namely, neglecting dissipation, voltage amplitude dynamics, and reactive power flows. Recently, there has been a common effort in trying to pursue a more realistic mathematical analysis of power grids, by incorporating reactive power flows [16, 17], voltage amplitude dynamics [54, 55], and dissipation [25, 26]. Despite all this work, there is still no clear extension of the winding partition to the full active-reactive power flows, even though there are some notable related preliminary works [56, 57]. Our results are an advance in the aforementioned collective effort.

To put our results in perspective with the resolution of the power flow equations, we solved both the Dissipative Flow Network Problem and the power flow equations on an adapted version of the IEEE-RTS96 test case [46, 58]. In Fig. 4, we compare synchronous states of the Kuramoto-Sakaguchi model (panels B and C, inner circle), with the corresponding solutions of the full power flow equations (panels B and C, outer annulus). We elaborate on the resolution of the full power flow equations in the Methods Section. First of all, one clearly sees that the main qualitative features (e.g., winding number, cohesiveness, clustering) of the power flow solutions are captured by the corresponding synchronous states of the Kuramoto-Sakaguchi model. Furthermore, it is remarkable that two solutions to the full power flow equations coexist, satisfying all voltage amplitude constraints as well as voltage angle stability. This example shows that loop flows and the winding partition are a fundamental features of power flow solutions. Our work is a contribution to the joint and long lasting effort in the quest an accurate mathematical analysis of power grids, which is a landmark in the area of power grids analysis.

We trust that the notion of winding partition has the potential to contribute elucidating many open problems in the fascinating phenomenon of synchronization in complex networks. We reiterate that even though we restricted our discussion to bidirected interactions for sake of clarity, the whole framework developed in this manuscript naturally applies to any system with directed interactions. Namely, our formalism is a first step towards a unified analysis of synchronization in any network of coupled oscillators, no matter the nature of the interactions.

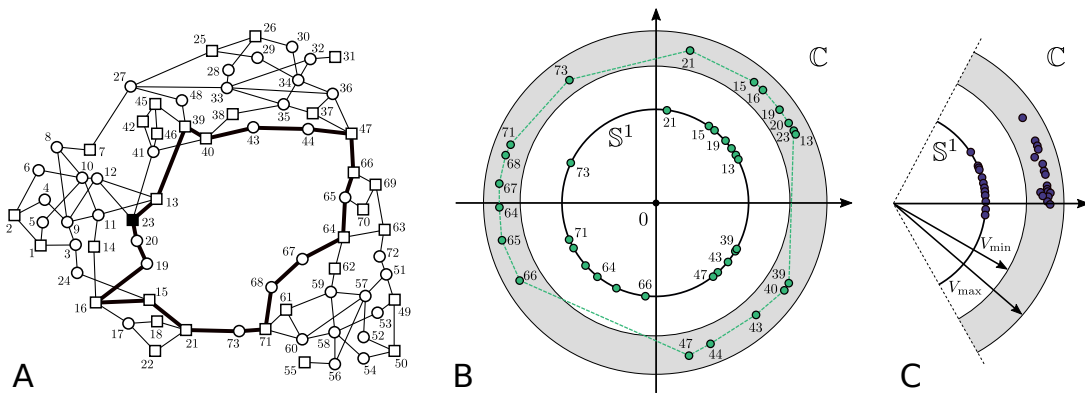


FIG. 4. Comparison of the power flow solutions and Kuramoto-Sakaguchi synchronous states on the IEEE RTS-96 test case [58]. (A) Geographic representation of the system. Circles are loads and squares are generators. The network is composed of $n = 73$ nodes, $m = 108$ edges, and therefore $c = 36$ independent cycles. The long cycle with thick edges is of particular interest, because its length promotes the existence of loop flows while keeping angular differences small (see Refs. [38, 39] for an extended discussion). (B, C) Combined representations of: (outer annulus) the complex voltages for solutions to the full power flow equations for an adapted version of the RTS-96 test case; (inner circle) the phase angles of synchronous states of the Kuramoto-Sakaguchi model on the same system. For sake of readability, only the values of the nodes around the long cycle of panel A are represented. The outer annulus represents the tolerated margin of variation for the voltage amplitudes in the power flow equations. The power flow solution in panel B has a nonzero winding number ($q = +1$) and there is a reasonable correspondence (ordering, clustering) between its voltage phases and the angles of the Kuramoto-Sakaguchi synchronous state. Similarly, both the power flow solution and the Kuramoto-Sakaguchi synchronous states in panel C have zero winding number, with all angles in relatively short arc. There are indeed two distinct solutions of the power flow equations on this version of the IEEE RTS-96 test case.

METHODS

We first provide the necessary grounds of directed and undirected graph theory, as well as a link between them. We refer to Ref. [15] for an extended discussion about graph and digraph theories. We then discuss the Kuramoto-Sakaguchi model and its link with the power flow equations.

Directed graphs.

A *directed graph* (or *digraph*) \mathcal{G}_d is the pair $(\mathcal{V}, \mathcal{E}_d)$ composed of a set of vertices (or nodes) $\mathcal{V} = \{1, \dots, n\}$ and a set of directed edges $\mathcal{E}_d \subset \mathcal{V} \times \mathcal{V}$, which are ordered pairs of vertices. For an edge $e = (i, j) \in \mathcal{E}_d$, i is the *source* of e , denoted s_e , and j is its *target*, denoted t_e , i.e., $e = (s_e, t_e)$. We denote the edge with opposite direction as $\bar{e} = (t_e, s_e)$. The existence of edges is encoded in the graph's *adjacency matrix*

$$(A_d)_{ij} = \begin{cases} 1, & \text{if } (i, j) \in \mathcal{E}_d, \\ 0, & \text{otherwise.} \end{cases} \quad (19)$$

The *out-degrees* (resp. *in-degrees*) are obtained as $\mathbf{d}^o = A_d \mathbf{1}$ (resp. $\mathbf{d}^i = A_d^\top \mathbf{1}$). The out- and in-degrees are gathered in the *out- and in-degree matrices* $D_o = \text{diag}(\mathbf{d}^o)$ and $D_i = \text{diag}(\mathbf{d}^i)$. We define the *Laplacian matrix* of \mathcal{G}_d as $L_d = D_o - A_d$. For a digraph with n vertices and

m directed edges, we define the $n \times m$ *incidence matrix*

$$(B_d)_{ie} = \begin{cases} 1, & \text{if } e = (i, j) \text{ for some } j, \\ -1, & \text{if } e = (j, i) \text{ for some } j, \\ 0, & \text{otherwise,} \end{cases} \quad (20)$$

which we decompose in positive and negative parts, referred to as *out-* and *in-incidence* matrices respectively,

$$B_o = [B_d]_+, \quad B_i = [B_d]_-, \quad (21)$$

such that $B_d = B_o - B_i$.

We notice the following relation, the fourth being unknown as far as we can tell.

Proposition 5. *The adjacency matrix A_d , the out- and in-degree matrices D_o and D_i , and the Laplacian matrix L_d of a directed graph can be written in terms of its out- and in-incidence matrices B_o and B_i :*

$$\begin{aligned} D_o &= B_o B_o^\top, & D_i &= B_i B_i^\top, \\ A_d &= B_o B_i^\top, & L_d &= B_o B^\top. \end{aligned} \quad (22)$$

Proof. The proofs for the adjacency matrix A_d and for the degree matrices D_o and D_i can be found in [59, Lem. 3.1 and Lem. 4.1]. The proof for the Laplacian matrix directly follows,

$$\begin{aligned} L_d &= D_o - A_d = B_o B_o^\top - B_o B_i^\top \\ &= B_o (B_o - B_i)^\top = B_o B^\top. \end{aligned} \quad (23)$$

□

Symbol	Name/Description
\mathcal{V}	Set of vertices.
\mathcal{G}, \mathcal{E}	Undirected graph, undirected edge set.
B, L	Incidence, and Laplacian matrices of an undirected graph [Eq. (24)].
C_Σ	cycle-edge incidence matrix of the set of cycles Σ [Eq. (26)].
$\mathcal{G}_d, \mathcal{E}_d$	Directed graph, set of directed edges.
\mathcal{G}_b	Bidirected counterpart of the undirected graph \mathcal{G} .
\mathcal{E}_b	Set of directed edges of the directed counterpart graph \mathcal{G}_b .
s_e, t_e	Source and target of edge e .
\bar{e}	Edge e with opposite direction.
d_i^o, d_i^i	Out- and in-degree of vertex i .
A_d, B_d, L_d	Adjacency, incidence, and Laplacian matrices of a digraph [Eqs. (19),(20)].
B_b	Incidence matrix of a bidirected graph.
B_o, B_i	Out- and in-incidence matrices of a digraph.
$\boldsymbol{\theta} = (\theta_1, \dots, \theta_n)^\top$	Vector of phase angles.
$\boldsymbol{\omega} = (\omega_1, \dots, \omega_n)^\top$	Vector of natural frequencies.
a_{ij}, ϕ	Coupling strength and phase frustration between nodes i and j .
γ_e	Bound on the angular difference over the edge e .
$h_e, h_{\bar{e}}$	Coupling functions over the edge e .
$h_{od,e}, h_{ev,e}$	Odd and even parts of the coupling over edge e [Eq. (12),(13)].
\mathbf{h}_γ	Extended flow function [Eq. (47)].
$R(\gamma)$	Domain of bounded angular differences [Eq. (9)].
\boldsymbol{q}_Σ	Winding map for the cycles in Σ [Eq. (4)].
$\Omega(\mathbf{u}; \Sigma)$	Winding cell with winding vector \mathbf{u} in the graph \mathcal{G} [Eq. (5)].
S_ϵ	Flow mismatch iteration [Eq. (11)].

TABLE I. List of symbols.

Remark. *The same proof is straightforwardly adapted to weighted directed graphs.*

Undirected graphs.

An (*undirected*) graph \mathcal{G} is a pair $(\mathcal{V}, \mathcal{E})$ composed of a set of n vertices (or nodes) $\mathcal{V} = \{1, \dots, n\}$ and a set of m edges, which are unordered pairs of vertices, $\mathcal{E} \subset \{\{i, j\} : i, j \in \mathcal{V}\}$. A *cycle* of \mathcal{G} is an ordered sequence of vertices $\sigma = (i_0, i_1, \dots, i_\ell = i_0)$, such that $\{i_j, i_{j+1}\} \in \mathcal{E}$ and $i_j \neq i_k$ for any $j, k \in \{1, \dots, \ell\}$.

Let us now choose an arbitrary orientation $[(i, j)$ or $(j, i)]$ for each undirected edge $\{i, j\} \in \mathcal{E}$. We can then define the *incidence matrix* of \mathcal{G} ,

$$B_{ie} = \begin{cases} 1, & \text{if } e = (i, j) \text{ for some } j, \\ -1, & \text{if } e = (j, i) \text{ for some } j, \\ 0, & \text{otherwise.} \end{cases} \quad (24)$$

The *Laplacian matrix* of \mathcal{G} can be computed as $L =$

BB^\top . Note that the incidence matrix is not unique and depends on the choice of edge orientations, whereas the Laplacian does not. Given a cycle $\sigma = (i_0, i_2, \dots, i_\ell)$, we define the *cycle vector* $\mathbf{v}_\sigma \in \{-1, 0, +1\}^m$, indexed by edges, as

$$(\mathbf{v}_\sigma)_e = \begin{cases} +1, & \text{if } e = (i_{k-1}, i_k) \text{ for some } k, \\ -1, & \text{if } e = (i_k, i_{k-1}) \text{ for some } k, \\ 0, & \text{otherwise.} \end{cases} \quad (25)$$

The *cycle space* of \mathcal{G} is the span of the cycle vectors of all cycles of \mathcal{G} , which is equivalently defined as the kernel of the incidence matrix B . A set of cycles $\Sigma = \{\sigma_1, \dots, \sigma_c\}$ is a cycle basis of \mathcal{G} if and only if the set of corresponding cycle vectors forms a basis of the cycle space.

Finally, given a cycle basis Σ of the graph \mathcal{G} , we define the *cycle-edge incidence matrix*,

$$C_\Sigma = (\mathbf{v}_{\sigma_1}, \dots, \mathbf{v}_{\sigma_c})^\top \in \mathbb{R}^{c \times m}. \quad (26)$$

Bidirected graphs

Dissipative couplings intrinsically require to distinguish the two orientations of each edge. Given an undirected graph $\mathcal{G} = (\mathcal{V}, \mathcal{E})$, its *bidirected counterpart* is the directed graph $\mathcal{G}_b = (\mathcal{V}, \mathcal{E}_b)$ with the same vertex set \mathcal{V} and where each undirected edge $\{i, j\} \in \mathcal{E}$ is doubled in the set of directed edges $(i, j), (j, i) \in \mathcal{E}_b$. A bidirected graph is a directed graph induced by an undirected graph.

If the undirected graph \mathcal{G} has incidence matrix $B \in \mathbb{R}^{n \times m}$ [Eq. (24)], then, with an appropriate indexing of the directed edges, the incidence matrix of \mathcal{G}_b can be written as $B_b = (B, -B) \in \mathbb{R}^{n \times 2m}$. Interestingly, we note that the Laplacian matrices of \mathcal{G} and \mathcal{G}_b are the same, namely (see Prop. 5),

$$L = BB^\top = L_b = B_o B_b^\top, \quad (27)$$

where the *out-incidence matrix* $B_o = [B_b]_+$ is the positive part of B_b . Notice that here,

$$B_o = ([B]_+, [B]_-). \quad (28)$$

The Kuramoto-Sakaguchi model

We illustrate the results of this manuscript with the *generalized Kuramoto-Sakaguchi model* [8, 23, 24],

$$\dot{\theta}_i = \omega_i - \sum_{j=1}^n a_{ij} [\sin(\theta_i - \theta_j - \phi) + \sin(\phi)], \quad (29)$$

for $i \in \{1, \dots, n\}$, where $\theta_i \in \mathbb{S}^1$ and $\omega_i \in \mathbb{R}$ are respectively the phase angle and the natural frequency of the i -th oscillator, $\phi \in (-\pi/2, \pi/2)$ is the *phase frustration* between oscillators, and $a_{ij} \in \mathbb{R}$ is the coupling strength

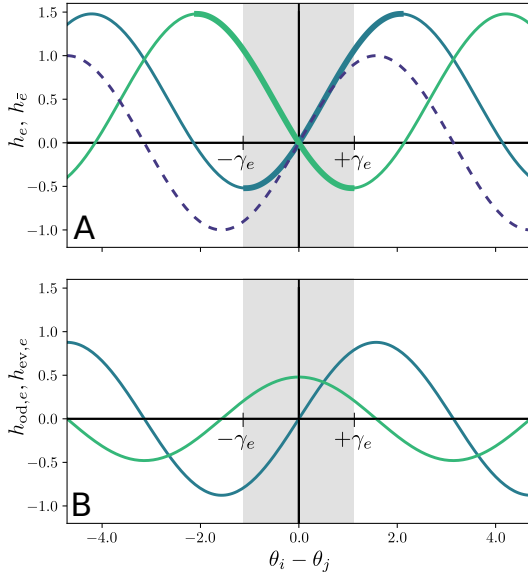


FIG. 5. (A) Comparison between coupling functions for Kuramoto [dashed dark blue, $h_e(x) = \sin(x)$] and Kuramoto-Sakaguchi [plain cyan, $h_e(x) = \sin(x - \phi) + \sin \phi$], with $\phi = 0.5$. The light green curve illustrates the coupling on the same edge, but with opposite orientation [$h_{\bar{e}}(-x) = \sin(-x - \phi) + \sin \phi$]. The thick parts (cyan and green) emphasize the region where the curve is increasing (resp. decreasing). The shaded gray area shows the interval where the coupling in both orientations is strictly monotone. (B) Odd (cyan) and even (green) parts of the Kuramoto-Sakaguchi coupling function, as defined in Eq. (17).

between oscillators i and j . The Kuramoto-Sakaguchi model directly translates to the framework of Eq. (1), with $h_{ij}(x) = \sin(x - \phi) + \sin \phi$, for all $e \in \mathcal{E}_b$, and is a natural extension of the original Kuramoto model, which is recovered for $\phi = 0$. The coupling function of the Kuramoto-Sakaguchi model is illustrated in Fig. 5A.

Remark. While in its original formulation, the Kuramoto-Sakaguchi model assumes homogeneous, all-to-all couplings, here we take the couplings to be given by an underlying network structure. For the sake of simplicity, in our examples we consider $a_{ij} = a_{ji}$ and $\phi_{ij} = \phi_{ji}$ for all connected nodes i and j . Nevertheless, we keep in mind that these assumptions are not necessary for our results and that our framework is adapted for much more general cases.

In order to illustrate some fundamental complications that arise in the Kuramoto-Sakaguchi model, compared to the original Kuramoto model, we detail two simple examples below.

Example (2-node system, vectorial form). Consider a system of two coupled Kuramoto-Sakaguchi oscillators with unit coupling and identical frustration, whose dy-

namics is given by

$$\begin{aligned} \dot{\theta}_1 &= \omega_1 - [\sin(\theta_1 - \theta_2 - \phi) + \sin \phi], \\ \dot{\theta}_2 &= \omega_2 - [\sin(\theta_2 - \theta_1 - \phi) + \sin \phi], \end{aligned} \quad (30)$$

with $\phi \in (-\pi/2, \pi/2)$.

In the Kuramoto model ($\phi = 0$), it is standard to write the dynamics in vectorial form as

$$\dot{\boldsymbol{\theta}} = \boldsymbol{\omega} - B \sin(B^\top \boldsymbol{\theta}), \quad (31)$$

where $B \in \mathbb{R}^{n \times m}$ is the incidence matrix of the (undirected) coupling graph of the system. In the Kuramoto-Sakaguchi model, this vectorial form is not that simple. Direct computation shows that writing

$$\dot{\boldsymbol{\theta}} = \boldsymbol{\omega} - B [\sin(B^\top \boldsymbol{\theta} - \phi \mathbf{1}_m) + \sin \phi \mathbf{1}_m], \quad (32)$$

does not yields the desired Eqs. (30).

In order to write this model in vectorial form, we need to distinguish the two orientation of each edge and consider \mathcal{G}_b , the bidirected counterpart of \mathcal{G} . One can verify that Eqs. (30) can be written as

$$\dot{\boldsymbol{\theta}} = \boldsymbol{\omega} - B_o [\sin(B_b^\top \boldsymbol{\theta} - \mathbf{1}_{2m} \phi) + \mathbf{1}_{2m} \sin \phi], \quad (33)$$

where B_o and B_b are the out-incidence matrix and the incidence matrix of the bidirected coupling graph.

Example (6-node cycle, sync. frequency). Let us consider six Kuramoto-Sakaguchi oscillators, coupled in a cycle, with identical, vanishing natural frequency, i.e.,

$$\dot{\theta}_i = -\sin(\theta_i - \theta_{i-1} - \phi) - \sin(\theta_i - \theta_{i+1} - \phi) + 2 \sin \phi, \quad (34)$$

for $i \in \{1, \dots, 6\}$, where we used periodic indexing. One straightforwardly verifies that $\boldsymbol{\theta}_0 = (0, \dots, 0)^\top$ is an equilibrium of Eq. (34) (and then a synchronous state).

One can also verify that the splay state $\boldsymbol{\theta}_1 = (0, -\pi/3, -2\pi/3, \pi, 2\pi/3, \pi/3)^\top$ is also a synchronous state. Indeed, in this case, Eq. (34) gives

$$\begin{aligned} \dot{\theta}_i &= -\sin(-\pi/3 - \phi) - \sin(\pi/3 - \phi) - 2 \sin \phi \\ &= 2 \cos(\pi/3) \sin \phi - 2 \sin \phi = -\sin \phi, \end{aligned} \quad (35)$$

independently of $i \in \{1, \dots, 6\}$. The state $\boldsymbol{\theta}_1$ is then synchronous, but it is an equilibrium only for the Kuramoto model ($\phi = 0$).

There are at least two main messages that can be taken from these examples. First, by extending our framework to directed graphs, we are able to write the Kuramoto-Sakaguchi model in vectorial form,

$$\dot{\boldsymbol{\theta}} = \boldsymbol{\omega} - B_o [\sin(B_d^\top \boldsymbol{\theta} - \phi) + \sin(\phi)]. \quad (36)$$

Note that a similar vectorial formulation of the Kuramoto-Sakaguchi model has recently been proposed

in Ref. [60], which, while more general than Eq. (36), does not provide as much insight in the underlying network structure.

Second, unlike the Kuramoto model, the average frequency of the system is not preserved along arbitrary trajectories. Also, if multiple synchronous states exist, then they have, in general, different synchronous frequencies. These claims are backed up by showing that the average frequency of the system depends on angular differences,

$$\sum_i \dot{\theta}_i = \sum_i \omega_i - \sum_{i,j} a_{ij} \sin \phi [1 - 2 \cos(\theta_i - \theta_j)], \quad (37)$$

which is time varying over the trajectories of the system, and not identical for different synchronous states.

On top of that, we reiterate that, contrary to the Kuramoto model, the Kuramoto-Sakaguchi model is not the gradient of any function (even locally). Therefore, the energy landscape approaches, valid for $\phi = 0$ [12, 22], are not directly applicable to $\phi \neq 0$.

The power flow equations

Under the assumption that voltage amplitudes are fixed, synchronous states of the Kuramoto-Sagauchi model are in direct correspondence with the solutions of the active *power flow equations* [12, 61]. The power flow equations relate the the balance of active (P_i) and reactive powers (Q_i) to the voltage amplitude (V_i) and phase (θ_i) at each node $i \in \{1, \dots, n\}$,

$$P_i = \sum_{j=1}^n V_i V_j [B_{ij} \sin(\theta_i - \theta_j) + G_{ij} \cos(\theta_i - \theta_j)], \quad (38)$$

$$Q_i = \sum_{j=1}^n V_i V_j [G_{ij} \sin(\theta_i - \theta_j) - B_{ij} \cos(\theta_i - \theta_j)], \quad (39)$$

with G_{ij} and B_{ij} being lines conductance and susceptance respectively. Defining

$$a_{ij} = V_i V_j \sqrt{B_{ij}^2 + G_{ij}^2}, \quad \phi_{ij} = \arctan(-G_{ij}/B_{ij}), \quad (40)$$

one verifies that solutions of Eq. (38) are steady states of Eq. (29).

Eqs. (38) and (39) are usually solved by iterative methods. In Fig. 4(B) and (C), outer annulus, we used a Newton-Raphson scheme [62, Sec. 6.4] with different, carefully chosen initial conditions to solve the full power flow equations on our version of the IEEE-RTS96 test case [58]. The squares are PV buses, the circles are PQ buses, and the slack bus is node 23. The synchronous states of the Kuramoto-Sakaguchi models were computed by the flow mismatch iteration S_ϵ [Eq. (11)], with $\epsilon = 0.01$.

DATA AVAILABILITY

All codes and data mentioned in the manuscript can be accessed online, in the DFNSolver repository [46].

CONTRIBUTIONS

All three authors designed the research; RD and SJ derived to the mathematical results; RD did the simulations; RD and FB analyzed the simulations and wrote the paper.

ACKNOWLEDGMENTS

RD was supported by the Swiss National Science Foundation, under grant number P400P2-194359. This work was partly supported by AFOSR grant FA9550-22-1-0059.

-
- [1] C. Huygens, *Oeuvres complètes de Christiaan Huygens*, edited by M. Nijhoff (Société hollandaise des sciences, 1993).
 - [2] A. Arenas, A. Díaz-Guilera, J. Kurths, Y. Moreno, and C. Zhou, “Synchronization in complex networks,” *Phys. Rep.* **469**, 93–153 (2008).
 - [3] S. H. Strogatz, “From Kuramoto to Crawford: exploring the onset of synchronization in populations of coupled oscillators,” *Physica D* **143**, 1–20 (2000).
 - [4] J. A. Acebrón, L. L. Bonilla, C. J. Pérez Vicente, F. Ritort, and R. Spigler, “The Kuramoto model: A simple paradigm for synchronization phenomena,” *Rev. Mod. Phys.* **77**, 137 (2005).
 - [5] A. T. Winfree, “Biological rhythms and the behavior of populations of coupled oscillators,” *J. Theoret. Biol.* **16**, 15–42 (1967).
 - [6] Y. Kuramoto, “Self-entrainment of a population of coupled non-linear oscillators,” in *Lecture Notes in Physics, vol. 39. International Symposium on Mathematical Problems in Theoretical Physics*, edited by Huzihiro Araki (Springer, Berlin, 1975) pp. 420–422.
 - [7] Y. Kuramoto, “Cooperative dynamics of oscillator community a study based on lattice of rings,” *Prog. Theor. Phys. Suppl.* **79**, 223–240 (1984).
 - [8] H. Sakaguchi, S. Shinomoto, and Y. Kuramoto, “Local and global self-entrainments in oscillator lattices,” *Prog. Theor. Phys.* **77**, 1005–1010 (1987).
 - [9] S. H. Strogatz and R. E. Mirollo, “Phase-locking and critical phenomena in lattices of coupled nonlinear oscillators with random intrinsic frequencies,” *Physica D* **31**, 143–168 (1988).
 - [10] H. Daido, “Lower critical dimension for populations of oscillators with randomly distributed frequencies: A renormalization-group analysis,” *Phys. Rev. Lett.* **61**, 231–234 (1988).

- [11] F. Dörfler and F. Bullo, “Synchronization in complex networks of phase oscillators: A survey,” *Automatica* **50**, 1539–1564 (2014).
- [12] F. Dörfler, M. Chertkov, and F. Bullo, “Synchronization in complex oscillator networks and smart grids,” *Proc. Natl. Acad. Sci. USA* **110**, 2005–2010 (2013).
- [13] D. A. Paley, N. E. Leonard, R. Sepulchre, D. Grunbaum, and J. K. Parrish, “Oscillator models and collective motion,” *IEEE Control Syst.* **27**, 89–105 (2007).
- [14] N. E. Leonard, T. Shen, B. Nabet, L. Scardovi, I. D. Couzin, and S. A. Levin, “Decision versus compromise for animal groups in motion,” *Proc. Natl. Acad. Sci. USA* **109**, 227–232 (2012).
- [15] F. Bullo, *Lectures on Network Systems*, 1st ed. (Kindle Direct Publishing, 2022).
- [16] J. W. Simpson-Porco, “A theory of solvability for lossless power flow equations – Part I: Fixed-point power flow,” *IEEE Trans. Control Netw. Syst.* **5**, 1361–1372 (2018).
- [17] J. W. Simpson-Porco, “A theory of solvability for lossless power flow equations – Part II: Conditions for radial networks,” *IEEE Trans. Control Netw. Syst.* **5**, 1373–1385 (2018).
- [18] S. Jafarpour, E. Y. Huang, K. D. Smith, and F. Bullo, “Flow and elastic networks on the n -torus: Geometry, analysis, and computation,” *SIAM Review* **64**, 59–104 (2022).
- [19] D. Aeyels and F. De Smet, “A mathematical model for the dynamics of clustering,” *Physica D* **237**, 2517–2530 (2008).
- [20] W. Xia and M. Cao, “Clustering in diffusively coupled networks,” *Automatica* **47**, 2395–2405 (2011).
- [21] K. Dvijotham and M. Chertkov, “Convexity of structure preserving energy functions in power transmission: Novel results and applications,” in *2015 American Control Conference (ACC)* (IEEE, Chicago, IL, USA, 2015) pp. 5035–5042.
- [22] S. Ling, R. Xu, and A. S. Bandeira, “On the Landscape of Synchronization Networks: A Perspective from Non-convex Optimization,” *SIAM J. Optim.* **29**, 1879–1907 (2019).
- [23] H. Sakaguchi and Y. Kuramoto, “A soluble active rotator model showing phase transitions via mutual entertainment,” *Prog. Theor. Phys.* **76**, 576–581 (1986).
- [24] H. Sakaguchi, S. Shinomoto, and Y. Kuramoto, “Mutual entrainment in oscillator lattices with nonvariational type interaction,” *Prog. Theor. Phys.* **79**, 1069–1079 (1988).
- [25] C. Balestra, F. Kaiser, D. Manik, and D. Witthaut, “Multistability in lossy power grids and oscillator networks,” *Chaos* **29**, 123119 (2019).
- [26] F. Hellmann, P. Schultz, P. Jaros, R. Levchenko, T. Kapitaniak, J. Kurths, and Y. Maistrenko, “Network-induced multistability through lossy coupling and exotic solitary states,” *Nat. Commun.* **11**, 592 (2020).
- [27] J. C. Bronski, T. Carty, and L. DeVille, “Configurational stability for the Kuramoto-Sakaguchi model,” *Chaos* **28**, 103109 (2018).
- [28] R. Berner, S. Yanchuk, Y. Maistrenko, and E. Schöll, “Generalized splay states in phase oscillator networks,” *Chaos* **31**, 073128 (2021).
- [29] A. Mihara and R. O. Medrano-T, “Stability in the Kuramoto-Sakaguchi model for finite networks of identical oscillators,” *Nonlin. Dyn.* **98**, 539–550 (2019).
- [30] Y. Zhang and A. E. Motter, “Symmetry-Independent Stability Analysis of Synchronization Patterns,” *SIAM Review* **62**, 817–836 (2020).
- [31] F. Battiston, G. Cencetti, I. Iacopini, V. Latora, M. Lucas, A. Patania, J.-G. Young, and G. Petri, “Networks beyond pairwise interactions: Structure and dynamics,” *Phys. Rep.* **874**, 1–92 (2020).
- [32] Y. Zhang, J. L. Ocampo-Espindola, I. Z. Kiss, and A. E. Motter, “Random heterogeneity outperforms design in network synchronization,” *Proc. Natl. Acad. Sci. USA* **118**, e2024299118 (2021).
- [33] M. H. Matheny, J. Emenheiser, W. Fon, A. Chapman, A. Salova, M. Rohden, J. Li, M. Hudoba de Badyn, M. Pósfai, L. Duenas-Osorio, M. Mesbahi, J. P. Crutchfield, M. C. Cross, R. M. D’Souza, and M. L. Roukes, “Exotic states in a simple network of nanoelectromechanical oscillators,” *Science* **363**, eaav7932 (2019).
- [34] D. M. Abrams and S. H. Strogatz, “Chimera states for coupled oscillators,” *Phys. Rev. Lett.* **93**, 174102 (2004).
- [35] D. M. Abrams, R. Mirollo, S. H. Strogatz, and D. A. Wiley, “Solvable model for chimera states of coupled oscillators,” *Phys. Rev. Lett.* **101**, 084103 (2008).
- [36] M. Wolfrum and O. E. Omel’chenko, “Chimera states are chaotic transients,” *Phys. Rev. E* **84**, 015201 (2011).
- [37] E. A. Martens, S. Thutupalli, A. Fourriere, and O. Hallatschek, “Chimera states in mechanical oscillator networks,” *Proc. Natl. Acad. Sci. USA* **110**, 10563–10567 (2013).
- [38] R. Delabays, T. Coletta, and Ph. Jacquod, “Multistability of phase-locking and topological winding numbers in locally coupled Kuramoto models on single-loop networks,” *J. Math. Phys.* **57**, 032701 (2016).
- [39] D. Manik, M. Timme, and D. Witthaut, “Cycle flows and multistability in oscillatory networks,” *Chaos* **27**, 083123 (2017).
- [40] R. P. Feynman, “Chapter II Application of Quantum Mechanics to Liquid Helium,” in *Progress in Low Temperature Physics*, Vol. 1 (Elsevier, 1955) pp. 17–53.
- [41] A. A. Abrikosov, “On the magnetic properties of superconductors of the second group,” *Sov. Phys. JETP* **5**, 1174 (1957).
- [42] A. J. Korsak, “On the question of uniqueness of stable load-flow solutions,” *IEEE Trans. Power App. Syst.* **91**, 1093–1100 (1972).
- [43] G. B. Ermentrout, “The behavior of rings of coupled oscillators,” *J. Math. Biol.* **23**, 55–74 (1985).
- [44] T. Coletta, R. Delabays, I. Adagideli, and P. Jacquod, “Topologically protected loop flows in high voltage AC power grids,” *New J. Phys.* **18**, 103042 (2016).
- [45] R. A. Horn and C. R. Johnson, *Matrix Analysis* (Cambridge University Press, New York, 1994).
- [46] R. Delabays, “DFNSolver: Dissipative Flow Networks Solver (v1.1), Zenodo,” (2022).
- [47] M. Fiedler, “Algebraic connectivity of graphs,” *Czech. Math. J.* **23**, 298–305 (1973).
- [48] Y. Tamura, H. Mori, and S. Iwamoto, “Relationship between voltage instability and multiple load flow solutions in electric power systems,” *IEEE Trans. Power App. Syst.* **102**, 1115–1125 (1983).
- [49] A. Klos and J. Wojcicka, “Physical aspects of the nonuniqueness of load flow solutions,” *Int. J. Elect. Power Energy Syst.* **13**, 268 – 276 (1991).
- [50] W. Ma and J. S. Thorp, “An efficient algorithm to locate all the load flow solutions,” *IEEE Trans. Power Syst.* **8**, 1077–1083 (1993).

- [51] D. Mehta, D. K. Molzahn, and K. Turitsyn, “Recent advances in computational methods for the power flow equations,” in *2016 American Control Conference (ACC)* (IEEE, Boston, MA, USA, 2016) pp. 1753–1765.
- [52] J. Casazza, “Blackouts: Is the risk increasing?” *Electr. World* **212**, 62 (1998).
- [53] S. G. Whitley, *Lake Erie Loop Flow Mitigation* (Technical Report; New York Independent System Operator, 2008).
- [54] J. W. Simpson-Porco, F. Dörfler, and F. Bullo, “Voltage collapse in complex power grids,” *Nat. Commun.* **7**, 10790 (2016).
- [55] K. Schmietendorf, O. Kamps, M. Wolff, P. G. Lind, P. Maass, and J. Peinke, “Bridging between load-flow and Kuramoto-like power grid models: A flexible approach to integrating electrical storage units,” *Chaos* **29**, 103151 (2019).
- [56] K. Dvijotham, M. Chertkov, and S. Low, “A differential analysis of the power flow equations,” in *2015 54th IEEE Conference on Decision and Control (CDC)* (IEEE, Osaka, 2015) pp. 23–30.
- [57] S. Park, R. Y. Zhang, J. Lavaei, and R. Baldick, “Uniqueness of Power Flow Solutions Using Monotonicity and Network Topology,” *IEEE Trans. Control Netw. Syst.* **8**, 319–330 (2021).
- [58] C. Grigg, P. Wong, P. Albrecht, R. Allan, M. Bhavaraju, R. Billinton, Q. Chen, C. Fong, S. Haddad, S. Kuruganty, W. Li, R. Mukerji, D. Patton, N. Rau, D. Reppen, A. Schneider, M. Shahidehpour, and C. Singh, “The IEEE Reliability Test System-1996. A report prepared by the Reliability Test System Task Force of the Application of Probability Methods Subcommittee,” *IEEE Trans. Power Syst.* **14**, 1010–1020 (1999).
- [59] C. Balbuena, D. Ferrero, X. Marcote, and I. Pelayo, “Algebraic properties of a digraph and its line digraph,” *J. Interconnect. Netw.* **4**, 377–393 (2003).
- [60] A. Arnaudon, R. L. Peach, G. Petri, and P. Expert, “Connecting Hodge and Sakaguchi-Kuramoto: a mathematical framework for coupled oscillators on simplicial complexes,” [arXiv preprint: 2111.11073](#) (2021).
- [61] J. Machowski, J. W. Bialek, and J. R. Bumby, *Power System Dynamics*, 2nd ed. (Wiley, Chichester, U.K, 2008).
- [62] A. R. Bergen and V. Vittal, *Power Systems Analysis* (Prentice Hall, 2000).
- [63] F. R. K. Chung, *Spectral Graph Theory*, CBMS Regional Conference Series in Mathematics ; Number 92 (Published for the Conference Board of the Mathematical Sciences by the American Mathematical Society, Providence, Rhode Island, 1997).
- [64] B. Mohar, “Eigenvalues, diameter, and mean distance in graphs,” *Graphs and Combin.* **7**, 53–64 (1991).
- [65] H. Sedrakyan and N. Sedrakyan, *Algebraic Inequalities*, Problem Books in Mathematics (Springer International Publishing, Cham, 2018).

SUPPLEMENTARY INFORMATION

Proof of Theorem 1

Without loss of generality, let us renumber the nodes such that node 1 is a leaf, and such that, for all $i \in \{2, \dots, n-1\}$, node i is a leaf of the subgraph $\mathcal{G}_i \subset \mathcal{G}$ where nodes with index up to $i-1$ are pruned. Furthermore, let us denote by e_i the unique edge that connects node $i \in \{1, \dots, n-1\}$ to the set of nodes $\{i+1, \dots, n\}$, and orient it such that $s_{e_i} = i$. The reversed edge is denoted $e_{i+m} = \bar{e}_i$. All directed edges are then indexed. This can be done iteratively and we provide an implementation of this renumbering in Ref. [46].

For convenience, we recall and slightly rephrase Eq. (10a)

$$\varphi = \omega_j - \sum_{\substack{e: \\ s_e=j}} h_e(\Delta_e), \quad j \in \{1, \dots, n\}, \varphi \in \mathbb{R}, \quad (41a)$$

$$|\Delta_e| \leq \gamma_e, \quad e \in \mathcal{E}. \quad (41b)$$

A solution Δ of Eq. (10a) is also a solution of Eqs. (41). Showing that there is at most one solution to Eqs. (41) then implies that there is at most one solution to Eq. (10a).

Assume that Δ and Δ' are two solutions of Eqs. (10a), with respective synchronous frequencies φ and φ' . Without loss of generality, assume that $\varphi \leq \varphi'$. We compare now the components of the two solutions recursively.

Initial step, $i = 1$. According to our choice of indexing, Eq. (41a) gives

$$h_{e_1}(\Delta_{e_1}) = \omega_1 - \varphi \geq \omega_1 - \varphi' = h_{e_1}(\Delta'_{e_1}), \quad (42)$$

and by monotonicity of the coupling functions,

$$\Delta_{e_1} \geq \Delta'_{e_1}. \quad (43)$$

Recursion step, $2 \leq i \leq n-1$. By the previous steps, we have $\Delta_{e_j} \geq \Delta'_{e_j}$ for $j \in \{1, \dots, i-1\}$. According to our choice of indexing, there is a single out-going edge from node i whose angle differences in the two solutions have not been compared, namely e_i (see Fig. 6). Again by Eq. (41a) and monotonicity of the coupling functions, we get

$$h_{e_i}(\Delta_{e_i}) = \omega_i - \sum_{\substack{e: s_e < i, \\ t_e = i}} h_{\bar{e}}(-\Delta_e) - \varphi \geq \omega_i - \sum_{\substack{e: s_e < i, \\ t_e = i}} h_{\bar{e}}(-\Delta'_e) - \varphi' = h_{e_i}(\Delta'_{e_i}), \quad (44)$$

and

$$\Delta_{e_i} \geq \Delta'_{e_i}. \quad (45)$$

Final step, $i = n$. All the previous steps together with Eq. (41a) and monotonicity of the coupling functions give

$$\varphi = \omega_n - \sum_{\substack{e: \\ t_e=n}} h_{\bar{e}}(-\Delta_e) \geq \omega_n - \sum_{\substack{e: \\ t_e=n}} h_{\bar{e}}(-\Delta'_e) = \varphi' \geq \varphi, \quad (46)$$

which implies $\varphi = \varphi'$. The inequalities in Eqs. (42), (43), (44), (45), and (46) are equalities and the two solutions are identical. Note that we crucially used that the coupling functions are strictly increasing. \square

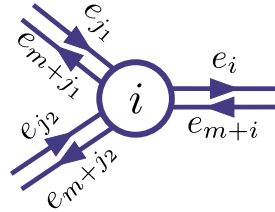


FIG. 6. Illustration of the node and edge indexing. In this example, our construction implies $j_1, j_2 < i \leq m$.

Proof of Theorem 3.

For technical purposes, we need to define the *extended flow function* $\mathbf{h}_\gamma: \mathbb{R}^m \rightarrow \mathbb{R}^{2m}$, for each edge e ,

$$[\mathbf{h}_\gamma(\mathbf{y})]_e = \begin{cases} h'_e(-\gamma_e)(y_e + \gamma_e) + h_e(-\gamma_e), & y_e < -\gamma_e, \\ h_e(y_e), & |y_e| \leq \gamma_e, \\ h'_e(\gamma_e)(y_e - \gamma_e) + h_e(\gamma_e), & y_e > \gamma_e, \end{cases} \quad (47)$$

$$[\mathbf{h}_\gamma(\mathbf{y})]_{e+m} = \begin{cases} -h'_{\bar{e}}(\gamma_e)(y_e + \gamma_e) + h_{\bar{e}}(\gamma_e), & y_e < -\gamma_e, \\ h_{\bar{e}}(-y_e), & |y_e| \leq \gamma_e, \\ -h'_{\bar{e}}(-\gamma_e)(y_e - \gamma_e) + h_{\bar{e}}(-\gamma_e), & y_e > \gamma_e, \end{cases} \quad (48)$$

which is well-defined and continuously differentiable.

Let $\xi, \eta \in \mathbb{R}^m$, such that $C_\Sigma \xi = C_\Sigma \eta = \mathbf{u} \in \mathbb{Z}^c$, and define $\mathbf{y} = \xi - \eta \in \text{Ker}(C_\Sigma)$. We construct the two diagonal $m \times m$ matrices $\Lambda_1(\xi, \eta)$, $\Lambda_2(\xi, \eta)$ as

$$(\Lambda_1)_e = (\xi_e - \eta_e)^{-1} \int_{\eta_e}^{\xi_e} (\mathbf{h}_\gamma)'_e(t) dt, \quad (49)$$

$$(\Lambda_2)_e = (\xi_e - \eta_e)^{-1} \int_{\eta_e}^{\xi_e} (\mathbf{h}_\gamma)'_{\bar{e}}(-t) dt. \quad (50)$$

We verify that

$$\mathbf{h}_\gamma(\xi) - \mathbf{h}_\gamma(\eta) = \begin{pmatrix} \Lambda_1 \\ -\Lambda_2 \end{pmatrix} (\xi - \eta) = \Lambda \cdot (\xi - \eta), \quad (51)$$

and the two matrices Λ_1, Λ_2 are nonnegative, because the coupling functions are assumed strictly increasing.

Then, by definition of S_ϵ ,

$$\|S_\epsilon(\xi) - S_\epsilon(\eta)\|_2^2 = \mathbf{y}^\top (I_m - \epsilon B^\top L^\dagger B_o \Lambda)^\top (I_m - \epsilon B^\top L^\dagger B_o \Lambda) \mathbf{y} = \|\mathbf{y}\|_2^2 - \epsilon \mathbf{y}^\top M \mathbf{y} + O(\epsilon^2), \quad (52)$$

where

$$M = B^\top L^\dagger B_o \Lambda + \Lambda^\top B_o^\top (L^\dagger)^\top B. \quad (53)$$

The remainder of the proof will be to show that, under the assumptions of the theorem, $\mathbf{y}^\top M \mathbf{y} > 0$. Then for $\epsilon > 0$ small enough, the second order term in Eq. (52) is dominated by the first order term, which is negative. Therefore, Eq. (52) is strictly smaller than $\|\mathbf{y}\|_2^2$, and S_ϵ is contracting.

We remark that $B_o \Lambda$ has exactly the same sparsity and sign pattern as B , with the difference being that the nonzero terms are not all the same, not even for the terms corresponding to the ends of a given edge. Namely,

$$(B_o \Lambda)_{ie} = \begin{cases} (\Lambda_1)_{ee}, & \text{if } e = (i, j) \text{ for some } j, \\ -(\Lambda_2)_{ee}, & \text{if } e = (j, i) \text{ for some } j, \\ 0, & \text{otherwise.} \end{cases} \quad (54)$$

We illustrate this property for a simple network in the box at page 16.

We now define

$$\Lambda_p = \frac{\Lambda_1 + \Lambda_2}{2}, \quad \Lambda_m = \frac{\Lambda_1 - \Lambda_2}{2}, \quad (55)$$

and recall that the out-incidence matrix is given by $B_o = ([B]_+, [B]_-)$ [Eq. (28)], where the square brackets denote the positive and negative parts (see the Methods Section for details). Then we can rewrite

$$B_o \Lambda = [B]_+ \Lambda_1 - [B]_- \Lambda_2 = [B]_+ (\Lambda_p + \Lambda_m) - [B]_- (\Lambda_p - \Lambda_m) = B \Lambda_p + |B| \Lambda_m, \quad (56)$$

with the absolute value taken elementwise.

Based on Eqs. (53) and (56), on the fact that $\mathbf{y} = B^\top L^\dagger B \mathbf{y}$ (see Prop. 6), and using $\mathbf{z} = L^\dagger B \mathbf{y}$, we compute

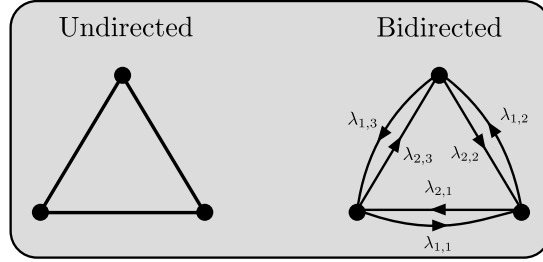
$$\mathbf{y}^\top M \mathbf{y} = \mathbf{z}^\top (B_o \Lambda B^\top + B \Lambda B_o^\top) \mathbf{z} = \mathbf{z}^\top (2B \Lambda_p B^\top + |B| \Lambda_m B^\top + B \Lambda_m |B|^\top) \mathbf{z} = 2\mathbf{z}^\top (L_p + D_m) \mathbf{z}, \quad (57)$$

Example. We illustrate Eq. (54) for the case of a triangular network:

$$B_o = \begin{pmatrix} 1 & 0 & 0 & 0 & 0 & 1 \\ 0 & 1 & 0 & 1 & 0 & 0 \\ 0 & 0 & 1 & 0 & 1 & 0 \end{pmatrix}, \quad \Lambda = \begin{pmatrix} \lambda_{1,1} & 0 & 0 \\ 0 & \lambda_{1,2} & 0 \\ 0 & 0 & \lambda_{1,3} \\ -\lambda_{2,1} & 0 & 0 \\ 0 & -\lambda_{2,2} & 0 \\ 0 & 0 & -\lambda_{2,3} \end{pmatrix}, \quad B_o \Lambda = \begin{pmatrix} \lambda_{1,1} & 0 & -\lambda_{2,3} \\ -\lambda_{2,1} & \lambda_{1,2} & 0 \\ 0 & -\lambda_{2,2} & \lambda_{1,3} \end{pmatrix},$$

and defining $\lambda_{p,i} = (\lambda_{1,i} + \lambda_{2,i})/2$ and $\lambda_{m,i} = (\lambda_{1,i} - \lambda_{2,i})/2$, we can write

$$B_o \Lambda = \begin{pmatrix} \lambda_{p,1} & 0 & -\lambda_{p,3} \\ -\lambda_{p,1} & \lambda_{p,2} & 0 \\ 0 & -\lambda_{p,2} & \lambda_{p,3} \end{pmatrix} + \begin{pmatrix} \lambda_{m,1} & 0 & \lambda_{m,3} \\ \lambda_{m,1} & \lambda_{m,2} & 0 \\ 0 & \lambda_{m,2} & \lambda_{m,3} \end{pmatrix} = B \Lambda_p + |B| \Lambda_m.$$



where

$$L_p = B \Lambda_p B^\top \quad (58)$$

$$D_m = (|B| \Lambda_m B^\top + B \Lambda_m |B|^\top) / 2. \quad (59)$$

First, notice that L_p is a weighted Laplacian matrix with the graph structure of \mathcal{G} . The weight of edge e is given by

$$(\Lambda_p)_{ee} = (\xi_e - \eta_e)^{-1} \int_{\eta_e}^{\xi_e} h'_{\text{od},e}(t) dt, \quad (60)$$

which, by the Mean Value Theorem, is bounded by

$$\inf_x h'_{\text{od},e}(x) \leq (\Lambda_p)_e \leq \sup_x h'_{\text{od},e}(x), \quad (61)$$

with the infimum and supremum taken over the admissible values of x . Therefore, by definition of the *odd weighted Laplacian matrix* [Eq. (14)], we can bound the second eigenvalue of L_p ,

$$\lambda_2(L_p) \geq \inf_{\mathbf{x}} \lambda_2(L_o(\mathbf{x})). \quad (62)$$

Finally, using that $\mathbf{z} = L^\dagger B \mathbf{y}$ is orthogonal to the null space of L_p ,

$$\mathbf{z}^\top L_p \mathbf{z} \geq \lambda_2(L_p) \|\mathbf{z}\|_2^2 \geq \inf_{\mathbf{x}} \lambda_2(L_o(\mathbf{x})) \|\mathbf{z}\|_2^2. \quad (63)$$

Second, let us break down the matrix D_m . Using the positive and negative parts of the incidence matrix, $B = [B]_+ - [B]_-$ and $|B| = [B]_+ + [B]_-$, direct computation shows

$$D_m = [B]_+ \Lambda_m [B]_+^\top - [B]_- \Lambda_m [B]_-^\top. \quad (64)$$

According to Prop. 5, we know that D_m is diagonal, and its elements can be computed as

$$(D_m)_{ii} = \sum_e ([B]_+)_{ie}^2 (\Lambda_m)_{ee} - \sum_e ([B]_-)_{ie}^2 (\Lambda_m)_{ee} = \sum_e ([B]_+ - [B]_-)_{ie} (\Lambda_m)_{ee} = \sum_{e \in E_i} \pm (\Lambda_m)_{ee}, \quad (65)$$

where E_i is the set of edges incident to node i in \mathcal{G} . Note that the elements of Λ_m are given by

$$(\Lambda_m)_e = (\xi_e - \eta_e)^{-1} \int_{\eta_e}^{\xi_e} h'_{\text{ev},e}(t) dt, \quad (66)$$

and, by the Mean Value Theorem, are bounded by

$$|(\Lambda_m)_e| \leq \sup_x |h'_{\text{ev},e}(x)|. \quad (67)$$

Therefore, by definition of the *even weighted degree* matrix [Eq. (15)], we can bound the elements of D_m ,

$$\min_i (D_m)_{ii} \geq -\sup_{\mathbf{x}, i} (D_e(\mathbf{x}))_{ii}, \quad (68)$$

which gives the bound

$$\mathbf{z}^\top D_m \mathbf{z} \geq \min_i (D_m)_{ii} \|\mathbf{z}\|_2^2 \geq -\sup_{\mathbf{x}, i} (D_e(\mathbf{x}))_{ii} \|\mathbf{z}\|_2^2. \quad (69)$$

To conclude, we introduce Eqs. (63) and (69) into Eq. (57), yielding

$$\mathbf{y}^\top M \mathbf{y} \geq \left[\inf_{\mathbf{x}} \lambda_2(L_o(\mathbf{x})) - \sup_{\mathbf{x}, i} (D_e(\mathbf{x}))_{ii} \right] \|\mathbf{z}\|_2^2, \quad (70)$$

which is strictly positive under the assumptions of the theorem. Going back to Eq. (52), we have shown that the first order term is strictly negative, and therefore, for $\epsilon > 0$ sufficiently small, the flow mismatch iteration S_ϵ is contracting, which concludes the proof. \square

Proposition 6. *Let \mathcal{G} be a graph and define its incidence matrix B , Laplacian matrix L , and the cycle-edge incidence matrix C_Σ (see the Methods Section for definitions). Then*

$$\text{Ker}(C_\Sigma) = \text{Ker}(I_m - B^\top L^\dagger B). \quad (71)$$

Proof. Let $\mathbf{x} \in \text{Ker}(I_m - B^\top L^\dagger B)$, then $\mathbf{x} = B^\top L^\dagger B \mathbf{x}$. We compute

$$C_\Sigma \mathbf{x} = C_\Sigma B^\top L^\dagger B \mathbf{x} = 0, \quad (72)$$

because $C_\Sigma B^\top = 0$. Thus $\text{Ker}(I_m - B^\top L^\dagger B) \subset \text{Ker}(C_\Sigma)$.

The rows of C_Σ are linearly independent by definition. Then its kernel has dimension $m - (m - n + 1) = n - 1$. The matrix $I_m - B^\top L^\dagger B$ is the orthogonal projection onto the kernel of B , therefore its rank is the nullity of B . By the Rank-Nullity Theorem,

$$\text{null}(I_m - B^\top L^\dagger B) = m - \text{null}(B) = n - 1. \quad (73)$$

The two kernel have the same dimension.

The set $\text{Ker}(I_m - B^\top L^\dagger B)$ is then a subspace of $\text{Ker}(C_\Sigma)$ and has the same dimension, they are then identical. \square

Bounds on the algebraic connectivity.

The following bounds are adapted from standard results of algebraic graph theory. We summarize the bounds of interest and the *ad hoc* quantities in Table II.

Proposition 7. *With the definition of L_o given in Eq. (14), we have the following bounds on its Fiedler eigenvalue:*

- (i) $\lambda_2 \geq 2c_e[1 - \cos(\pi/n)]$ [47, 4.3];
- (ii) $\lambda_2 \geq (nD_{i,\min})^{-1}$ (adapted from [63, Lemma 1.9]);
- (iii) $\lambda_2 \geq 4 \min_e \sigma_{\min,e}/nD$ (adapted from [64, Theorem 4.2]).

All relevant quantities are defined in Tab. II.

Proof. (i). Defining the *weighted edge connectivity* [47]

$$c(\mathbf{x}) = \min_{\mathcal{S}} \sum_e h'_{\text{od},e}(x_e), \quad (74)$$

where the minimum is taken over subsets of edges $\mathcal{S} \subset \mathcal{E}$ that split the graph \mathcal{G} , we can adapt the proof of [47, 4.3], yielding

$$\lambda_2(L_o) \geq 2c(\mathbf{x}) [1 - \cos(\pi/n)] \geq 2c_e [1 - \cos(\pi/n)], \quad (75)$$

independently of \mathbf{x} , where c_e is defined in Tab. II.

(ii). We adapt here the proof of [63, Lem. 1.9]. Let \mathbf{v} be the eigenvector of L_o associated with λ_2 and assume that $|v_i| = \max_k |v_k|$ (recall that all these quantities depend on \mathbf{x}). Because L_o is a symmetric Laplacian matrix, $\mathbf{1}^\top \mathbf{v} = 0$ and there is an index j such that $v_i v_j < 0$. We denote with P_{ij} the shortest (weighted) path from i to j . Now,

$$\lambda_2 = \frac{\mathbf{v}^\top L_o \mathbf{v}}{\mathbf{v}^\top \mathbf{v}} = \frac{\sum_{e=(k,\ell)} h'_{\text{od},e}(x_e) (v_k - v_\ell)^2}{\sum_k v_k^2} \geq \sum_{e=(k,\ell) \in P_{ij}} \frac{h'_{\text{od},e}(x_e) (v_k - v_\ell)^2}{n v_i^2}. \quad (76)$$

Defining the *odd weighted diameter*

$$D_w(\mathbf{x}) = \max_{i,j} \min_{P_{ij}} \sum_{e \in P_{ij}} [h'_{\text{od},e}(x_e)]^{-1}, \quad (77)$$

where the maximum is taken over all pairs of vertices and the minimum is taken over all simple paths joining i and j , we can apply the Sedrakyan inequality [65, Ch. 8] (direct consequence of the Cauchy-Schwarz inequality) to the numerator and get

$$\lambda_2 \geq \frac{[D_w(\mathbf{x})]^{-1} (v_i - v_j)^2}{n v_i^2} \geq \frac{1}{n D_w(\mathbf{x})} \geq \frac{1}{n d_w}, \quad (78)$$

where d_w is defined in Tab. II.

(iii). Alternatively, both sides of the identity

$$\mathbf{v}^\top L_o \mathbf{v} = \lambda_2 \mathbf{v}^\top \mathbf{v}, \quad (79)$$

can be bounded as follows,

$$\mathbf{v}^\top L_o \mathbf{v} = \sum_{e=(i,j) \in \mathcal{E}} h'_{\text{od},e}(x_e) (v_i - v_j)^2 \geq \min_e \sigma_{\text{min},e}, \quad (80)$$

and

$$\begin{aligned} 2n \mathbf{v}^\top \mathbf{v} &= \sum_i \sum_j (v_i - v_j)^2 \leq \sum_i \sum_j |P_{ij}| \sum_{(k,\ell) \in P_{ij}} (v_k - v_\ell)^2 \leq \sum_{(k,\ell) \in \mathcal{E}} (v_k - v_\ell)^2 d_{\mathcal{G}} \sum_i \sum_j \chi_{ij}(k,\ell) \\ &\leq \sum_{(k,\ell) \in \mathcal{E}} (v_k - v_\ell)^2 d_{\mathcal{G}} n^2 / 2, \end{aligned} \quad (81)$$

where we used that $\mathbf{v}^\top \mathbf{1} = 0$ and the Cauchy-Schwartz inequality at the first line, P_{ij} is a chosen (unweighted) shortest path between i and j , $\chi_{ij}(e)$ is its indicator function, and we used [64, Lemma 4.1] at the last inequality. Plugging these bounds together yields

$$2n \min_e \sigma_{\text{min},e} \leq \lambda_2 d_{\mathcal{G}} n^2 / 2, \quad (82)$$

which concludes the proof. \square

Bounds	Reference
$\max_i (D_e)_{ii} \leq \max_i \sum_{e \in E_i} \alpha_{\max,e}$	Direct computation (E_i is the set of edges incident to node i).
$\lambda_2 \geq 2c_e [1 - \cos(\pi/n)]$	Prop. 7, adapted from [47, 4.3].
$\lambda_2 \geq (nd_w)^{-1}$	Prop. 7, adapted from [63, Lemma 1.9].
$\lambda_2 \geq 4 \min_e \sigma_{\min,e} / nd_{\mathcal{G}}$	Prop. 7, adapted from [64, Theorem 4.2].
Definitions	Name
$\alpha_{\max,e} = \sup_x h'_{\text{ev},e}(x) $	Maximal even slope.
$\sigma_{\min,e} = \inf_x h'_{\text{od},e}(x)$	Minimal odd slope.
$c_e = \min_{E \subset S} \sum_{e \in E} \sigma_{\min,e}$	Minimized odd weighted edge connectivity (S is the set of splitting edge sets).
$d_w = \max_{i,j} \min_{P_{ij}} \sum_{e \in P_{ij}} \sigma_{\min,e}^{-1}$	Maximized odd weighted diameter (P_{ij} denotes a path between i and j).
$d_{\mathcal{G}} = \max_{i,j} \min_{P_{ij}} P_{ij} $	Graph diameter (P_{ij} denotes a path between i and j).

TABLE II. List of bounds on the components of Eq. (18) and definition of the *ad hoc* quantities. Note that all quantities are independent of the state of the system and can be determined beforehand.